PNAS RESEARCH ARTICLE | EARTH, ATMOSPHERIC, AND PLANETARY SCIENCES OPEN ACCESS

Cloud transition across the daily cycle illuminates model responses of trade cumuli to warming

Jessica Vial[a,1], Anna Lea Albright[a], Raphaela Vogel[a,b], Ionela Musat[a], and Sandrine Bony[a]

Edited by Kerry Emanuel, Massachusetts Institute of Technology, New Harbor, ME; received June 7, 2022; accepted December 16, 2022

The response of trade cumulus clouds to warming remains a major source of uncertainty for climate sensitivity. Recent studies have highlighted the role of the cloud–convection coupling in explaining this spread in future warming estimates. Here, using observations from an instrumented site and an airborne field campaign, together with high-frequency climate model outputs, we show that i) over the course of the daily cycle, a cloud transition is observed from deeper cumuli during nighttime to shallower cumuli during daytime, ii) the cloud evolution that models predict from night to day reflects the strength of cloud sensitivity to convective mass flux and exhibits many similarities with the cloud evolution they predict under global warming, and iii) those models that simulate a realistic cloud transition over the daily cycle tend to predict weak trade cumulus feedback. Our findings thus show that the daily cycle is a particularly relevant testbed, amenable to process studies and anchored by observations, to assess and improve the model representation of cloud–convection coupling and thus make climate projections more reliable.

trade-wind cumulus | daily cycle | low-cloud feedback | general circulation models | observations

Significance

The response of trade-wind clouds to warming has long been a major source of uncertainty for climate change projections. By analyzing a set of climate models, we identify two contrasting types of model behaviors, which are evident both at the daily timescale and under global warming. These opposing behaviors depend on whether models can simulate cloud transitions—between very shallow and deeper cumuli—in response to changes in the convective mass flux. We show that the daily cycle can be used as a laboratory for assessing the physical credibility of trade cumulus responses to warming as simulated by climate models relative to observed cloud variations and processes. Our findings can also help guide future model development using observational benchmarking.

It is long-established that uncertainty in the response of clouds to warming leads to large uncertainty in the magnitude of the ultimate global warming. One approach to untangling this persistent uncertainty is to examine cloud responses in individual regimes and link these cloud responses to a physical hypothesis that can be tested using observations. Despite the apparent simplicity of this framework, formulating—and eventually falsifying—a specific physical hypothesis that can explain the diversity of cloud behaviors across models and observations remains difficult but not impossible. For extratropical low clouds for instance, recent studies used observational constraints on supercooled liquid droplets and cloud glaciation rates to provide evidence for less negative extratropical cloud feedback in mixed-phase clouds (1–3). The spread of trade cumulus feedback has long been a major source of uncertainty for climate sensitivity (4–7). Moreover, the large sensitivity of trade cumuli to environmental changes predicted by some General Circulation Models (GCMs) (8) seems at odds with the small sensitivity of trade cumuli to surface warming inferred from satellite observations at the interannual timescale (7, 9) or predicted by high-resolution numerical models in idealized experiments (10, 11). The diversity and uncertainty of trade cumulus feedback across models are thought to relate to the representation of the strength of cloud–convection coupling (12–21). Measurements from the recent EUREC^{4}A (Elucidating the Role of Cloud-Circulation Coupling in Climate) field campaign (22, 23) demonstrated that i) the cloud–convection coupling observed in nature is stronger than what is simulated by most climate models, and ii) models with no or weak cloud–convection coupling exhibit a larger sensitivity of cloud-base cloud fraction to relative humidity than to convection, and they simulate more positive trade cumulus cloud feedback under global warming (21). Climate models with weaker cloud–convection coupling are thus less credible with respect to observational constraints, falsifying an important line of evidence in support of a large trade cumulus feedback and high climate sensitivity (14, 16, 18).

An ensuing question is how to physically assess the strength of this cloud–convection coupling and guide future model development. Past studies showed that trade-wind cumulus clouds exhibit strong daily variations in the vertical profile of cloudiness, likely driven by variations in the intensity of shallow convection (24). The trade-wind daily cycle exhibits an evolution of two populations of shallow clouds (with a maximal depth of 3 to 4 km, i.e., below the freezing level): a population of nonprecipitating very shallow clouds maximizing during daytime and a population of precipitating deeper clouds maximizing during nighttime as convection strengthens (24, 25). These results raise the possibility that the daily cycle could be a natural laboratory for quantifying the coupling between convection and trade cumulus amount in models and observations.

Author affiliations: [a]Laboratoire de Météorologie Dynamique Institut Pierre Simon Laplace (LMD IPSL), Sorbonne Université, CNRS, 75005 Paris, France; and [b]University of Hamburg, 20148 Hamburg, Germany

Author contributions: J.V. and S.B. designed research; I.M. performed model simulations; J.V. performed research; I.M. contributed new reagents/analytic tools; J.V., A.L.A., and R.V. analyzed data; and J.V., A.L.A., R.V., and S.B. wrote the paper.

The authors declare no competing interest.

This article is a PNAS Direct Submission.

[1]To whom correspondence may be addressed. Email: jessica.vial@lmd.ipsl.fr.

This article contains supporting information online at http://www.pnas.org/lookup/suppl/doi:10.1073/pnas.2209805120/-/DCSupplemental.

Published February 13, 2023.

This work focuses on the changing occurrence of shallower and deeper trade-wind cloud populations; what we subsequently call "a daily cloud transition". We demonstrate that the transition between very shallow and deeper low clouds occurring over the daily cycle is a useful testbed for assessing cloud–convection coupling in climate models. The daily cycle provides a daily opportunity to collect observations and forms a substantial observational testbed. Here, we focus on the Barbados region, using 10 y of ground-based remote sensing observations from the Barbados Cloud Observatory [BCO, (17)] and extensive airborne measurements from the EUREC^{4}A field campaign (22, 23). In particular, we show that the daily transition from very shallow to deeper clouds reflects the strength of the cloud–convection coupling and that this cloud transition at the daily timescale discriminates among trade cumulus feedback under global warming. Daily cloud transitions thus provide a framework for developing model physics in a way that is directly relevant for evaluating the credibility of simulated low-cloud feedback.

Daily Cycle of the Trade-Wind Boundary Layer

Cloudiness from Models and Observations. We use 10 y of winter-time cloud radar observations from the BCO to construct a reference daily cycle of trade-wind clouds (*Materials and Methods*). Consistently with previous studies (24, 26), the overall cloudiness is lowest during daytime, while clouds deepen during nighttime and CF maximizes before sunrise (Fig. 1*A*). Around the cloud-base level, the daily variability is significant (~20% with respect to the daily mean value) and almost exclusively driven by

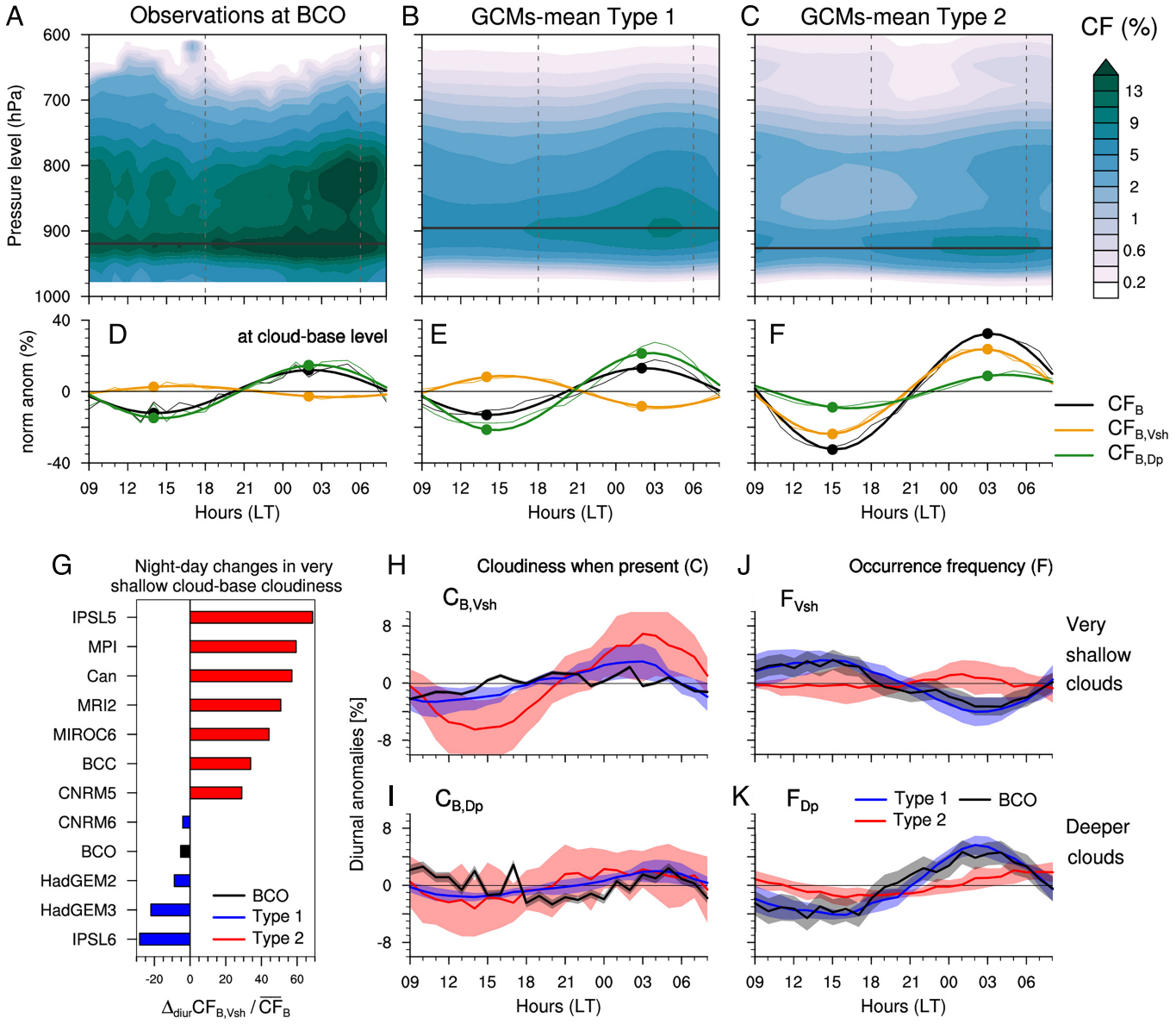

Fig. 1. Two contrasted daily cycles of trade-wind cloudiness. Mean daily cycle of the CF vertical distribution for (*A*) radar observations from BCO, (*B*) type 1 and (*C*) type 2 multimodel mean, with the mean cloud-base level represented as the black horizontal line. (*D–F*) CF_B daily anomalies normalized by daily mean ($\overline{CF}_B$) for all clouds with cloud-top below a 600-hPa level (CF_B, black), very shallow clouds with cloud-top below a 850-hPa level ($CF_{B,Vsh}$, orange) and deeper clouds with cloud-top between 850 and 600 hPa ($CF_{B,Dp}$, green). The first harmonic is superimposed on thicker lines, and the minimum and maximum CF_B are indicated by the colored markers. (*G*) Changes in $CF_{B,Vsh}$ between times of maximum and minimum CF_B normalized by $\overline{CF}_B$. (*H* and *I*) Daily anomalies of CF_B when either the very shallow or deeper cloud population is present (*C*), with the solid line and shading representing the multiday mean and SE (for BCO, black) and the multimodel mean and SD (for type 1, blue, and type 2, red), respectively. (*J* and *K*) Same as (*H* and *I*) but for the occurrence frequency of the cloud populations (*F*).

deeper clouds with cloud tops between 850 and 600 hPa (~1.3 to 4 km). In contrast, very shallow clouds (below the 850-hPa level), exhibit a weak daily cycle in their cloud coverage, maximizing during daytime (Fig. 1*D*).

All models qualitatively represent the overall daily cycle in cloudiness, with an increase in CF and cloud depth overnight and a minimum in the afternoon (Fig. 1 *B* and *C*). The amplitude of this daily cycle is, however, very diverse among individual models (*SI Appendix*, Fig. S1). We identify two types of model behaviors differing in their ability to represent the relative contributions of the very shallow and deeper cloud populations to the daily cycle at the cloud-base level (Fig. 1 *E*–*G*). Models of type 1 exhibit a nighttime increase of cloud-base cloud fraction (CF_B) mainly due to deeper clouds, while the very shallow cloud contribution is negative (i.e., dominant during daytime), consistent with the BCO observations. In contrast, for models of type 2, both cloud populations vary in phase across the daily cycle, with the very shallow clouds contributing 30 to 70% to the daily amplitude of CF_B (Fig. 1*G*). That is, all models qualitatively reproduce the daily cycle of CF_B, but type 2 models reproduce it for erroneous reasons, as the nighttime maximum in cloud fraction is accomplished by very shallow clouds instead of by deeper clouds.

Changes in CF_B can either be due to changes in cloud amount when a given population is present (*C*) or due to changes in the occurrence frequency of the cloud population (*F*). Fig. 1 *H*–*K* show that in the observations and type 1 models, CF_B changes arise from a daily transition between the very shallow and the deeper cloud populations (*J* and *K*). Type 1 models exhibit a remarkably realistic behavior as compared to BCO, with an increased occurrence of deeper clouds overnight at the expense of very shallow clouds. Type 2 models, in contrast, barely capture this cloud transition (i.e., weak and out-of-phase daily cycle in the occurrence frequency of cloud populations), without this being particularly linked to a lack of one of the two cloud populations (*SI Appendix*, Table S1). Instead, the daily cycle at cloud base is largely driven by changes in cloudiness for a given population (*H* and *I*). The question now arises as to what processes are needed in the models to simulate this observed cloud transition.

Convective Control on the Cloud Transition. The trade cumulus daily cycle is independent of sea surface temperature (SST) variations, which are weak in this region of relatively strong and sustained surface winds (24). Island effects, such as land/sea breezes, are also negligible (26). The daily cycle can be interpreted as a result of a nighttime increase in surface winds (26, 27) and buoyancy fluxes (25) and/or a nighttime increase in the radiatively driven instability across the depth of the cloud layer (28), each of which can reinforce the turbulent and convective transports of heat and moisture within the boundary layer. However, depending on the model, the relative contribution of convective and turbulent transports to the total subgrid-scale transport may differ, which can, in turn, lead to differences in simulated cloud fraction and cloud depth.

The daily cycle in surface turbulent fluxes, lower tropospheric stability, and large-scale subsiding motion is similar in both types of models (*SI Appendix*, Fig. S2). Yet, different behaviors arise between the two groups of models when considering the turbulent and convective tendencies in moist static energy (MSE)—used here to diagnose subgrid-scale transports (Fig. 2 and *SI Appendix*, Figs. S3, S4 and *Text*). In type 1 models, the level of maximum total subgrid-scale transport (a proxy for transport depth) evolves from below cloud base during daytime to the upper cloud layer during nighttime (black markers in Fig. 2*A* and *SI Appendix*, Figs. S3 and S4). This nighttime deepening of the subgrid-scale transport is primarily accomplished by convection (Fig. 2*A* and *SI Appendix*, Fig. S4) and is associated with reduced net moistening near the cloud-base level owing to a

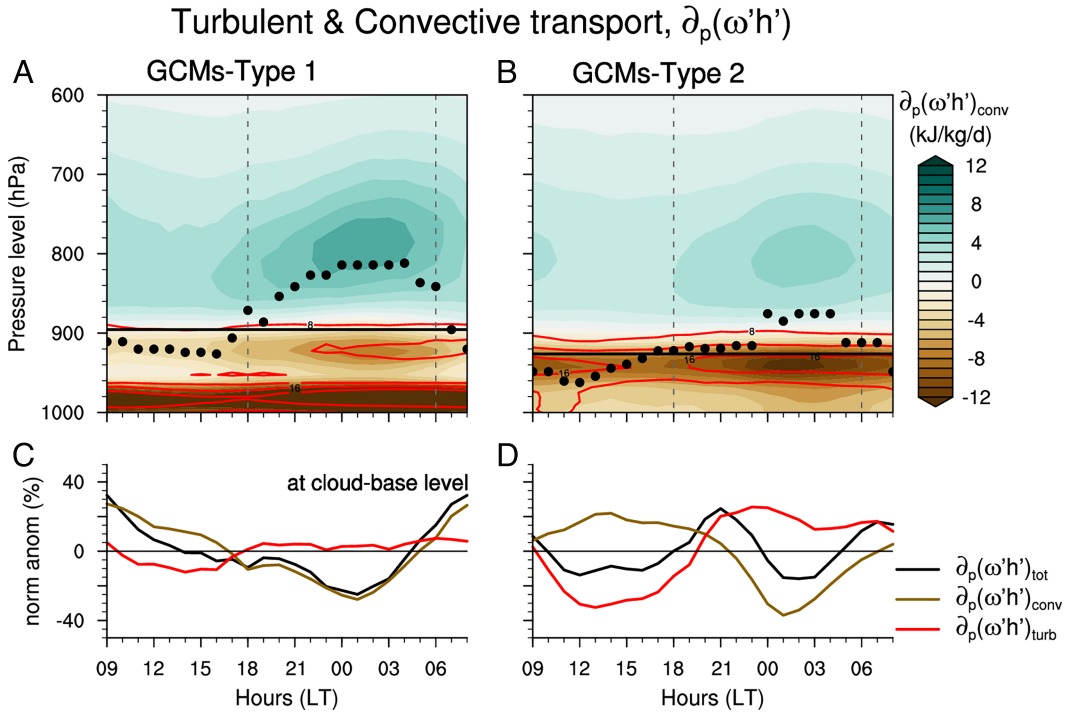

Fig. 2. Cloud transition mediated by convective transport. (*A* and *B*) Daily cycle in convective transport, defined as the moist static energy (MSE) tendency due to parameterized convection (shading) for (*A*) type 1 and (*B*) type 2 models, with mean cloud-base level (black horizontal line). Red contours show the MSE tendency due to turbulence (from 8 to 20 by 4 kJ/kg/d). Black markers indicate the level of maximum total subgrid-scale transport (from convection and turbulence; *SI Appendix*, Fig. S3). (*C* and *D*) Daily anomalies at cloud base of the total subgrid-scale transport (black), convective transport (brown), and turbulent transport (red).

stronger contribution of convective drying relative to turbulent moistening at the lowest levels (Fig. 2*C* and *SI Appendix*, Fig. S4). In type 2 models, the daily cycles in subgrid-scale transports are more diverse among individual models (*SI Appendix*, Figs. S3, and S4), but some common features nevertheless emerge. Specifically, a large part of the total subgrid-scale transport is accomplished by turbulence. This turbulent transport maximizes at the cloud-base level in all type 2 models (red contours in Fig. 2*B* and *SI Appendix*, S4), explaining why in these models the total mixing tends to be confined to low levels, around cloud base (black markers in Fig. 2*B*), with nighttime moistening at cloud base—when turbulence dominates—in most models of this group (Fig. 2*D* and *SI Appendix*, S4). The significant moisture source at the cloud-base level from surface-based turbulent transport (seen for type 2 models) is more expected to occur in stratocumulus or stratocumulus-to-cumulus transition regimes (29). Therefore, type 2 models tend to represent clouds that are closer to stratocumulus, which are known to exhibit greater variability in cloud fraction in response to changes in large-scale environmental conditions than trade-wind cumulus clouds (7–9), and as will be shown later (Figs. 3 *B* and *C* and 4*B*).

Overall, the dominant influence of the convective transport in type 1 models partly explains the greater ability of these models to produce transitions from very shallow to deeper clouds. More specifically, all models predict an enhanced MSE source overnight due to increased surface wind speed and heat fluxes, but the two groups of models predict different responses of the vertical transport and clouds: In type 1 models, the response is an enhanced vertical transport of MSE by convection and cloud deepening, whereas in most type 2 models (in which the vertical MSE transport is primarily accomplished by turbulence), the cloud depth remains approximately unchanged and the cloud fraction responds to low-level moistening.

Note that some type 2 models actually predict some daily variability in the convective transport but no cloud transition. It is because in these models, the parameterization of low-level clouds is not properly coupled to convective processes. This is illustrated by the IPSL5 model (The model's original name and reference are provided in *SI Appendix*, Table S1), in which clouds are more strongly dependent on the grid-scale degree of saturation than on convective fluctuations (30), despite the apparent coupling between the cloud and convection parameterization schemes (*SI Appendix*, Table S2). In the next section, we show how the models' representation of the daily cycle also connect to systematic model behaviors of the coupling between clouds and convection.

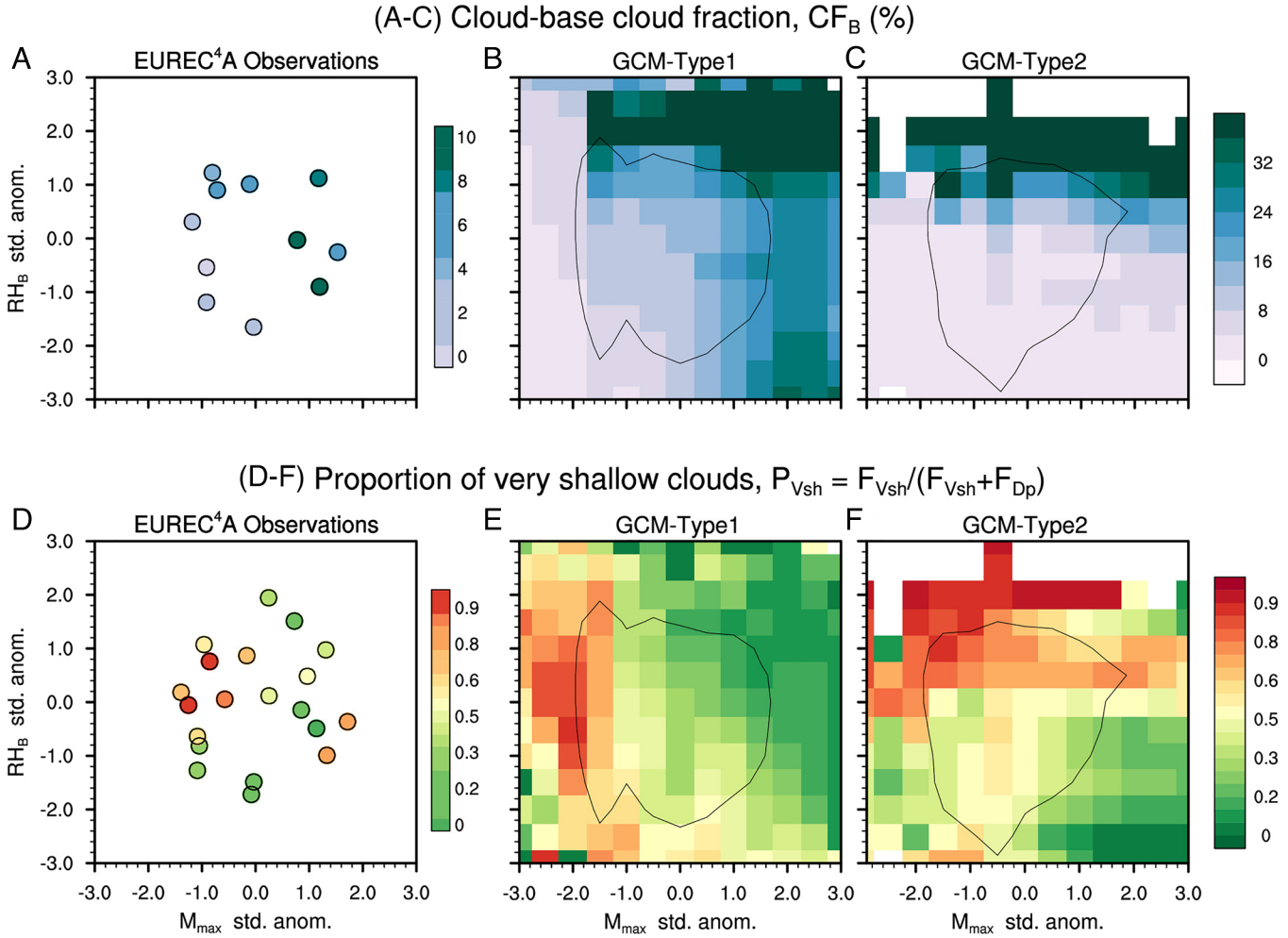

Fig. 3. Relative dependence of clouds on convective mass flux and relative humidity. (*A–C*) CF_B composited as a function of binned standardized anomalies of the convective mass flux maximum below the 850-hPa level and the relative humidity at the cloud-base level for (*A*) EUREC^{4}A data and aggregated (*B*) type 1 and (*C*) type 2 models. (*D–F*) Same as (*A–C*) but for the proportion of very shallow clouds among all shallow clouds (P_{Vsh}). About 90% of the data are contained within the black perimeter.

Convective vs. Relative Humidity Controls on Clouds

Despite a large diversity of cloud parameterizations in GCMs (*SI Appendix*, Table S2), the fractional cloud coverage always depends on the mean degree of saturation of the grid box (often through relative humidity (RH) or saturation deficit) and on subgrid-scale fluctuations (most often associated with turbulence and/or convection) of humidity or another moist thermodynamic variable. Here, we assess the degree to which clouds are coupled to convection, by binning cloudiness as a function of the convective mass flux (M) maximum (a proxy for convective intensity) and mean RH at the cloud-base level (Fig. 3). Two aspects of the simulated cloudiness are examined: CF_B and the proportion of very shallow clouds relative to all shallow clouds (P_{Vsh}), which is used as a diagnostic of the transition between the very shallow and deeper cloud populations. We use all hourly model outputs to construct these composites, which we evaluate against observed hourly covariability between clouds, mass flux, and relative humidity from the EUREC^{4}A field campaign (*Materials and Methods* and ref. 21).

Shallow cumuli near Barbados depend on both convective mass flux and relative humidity, although the former has twice as much control over CF_B as RH (Fig. 3 *A* and *D*, see also ref. 21). Overall, with increased mass flux, clouds deepen with enhanced coverage near the base level. Furthermore, at lower convective intensities, increased humidity is accompanied by cloud shallowing and a slight increase in CF_B.

None of the models perfectly reproduces this observed relationship among clouds, convection, and humidity. The two groups of models (which, as shown earlier, relate to distinct daily cloud transitions) exhibit contrasted behaviors, with type 2 models being the most distinct from observations. In type 2 models, CF_B systematically increases with higher RH and depends only weakly on convection (Fig. 3*C* and *SI Appendix*, S5). Moreover, CF_B can exhibit large variations with relative humidity, often close to the upper bound of the model's humidity distribution. This behavior (particularly pronounced for BCC, Can4, MPI, and IPSL5) is reminiscent of an "all-or-nothing" behavior in which CF depends only on the domain-averaged degree of saturation (for instance Figure 1 in ref. 30). Fig. 3 *D*–*F* confirms that the ability of models to produce cloud transitions is related to the strength of the cloud–convection coupling. Type 1 models exhibit a somewhat more realistic behavior as compared to EUREC^{4}A. With enhanced mass flux, the cloud deepening transitions are more pronounced and associated with less abrupt and smaller changes in CF_B (Fig. 3 *B* and *E*), which also suggests that clouds depend more on the subgrid-scale variability than on the grid-scale degree of saturation. Type 1 models, however, tend to underestimate the dependence of P_{Vsh} on RH for small mass flux values (Fig. 3*E* and *SI Appendix*, S6).

Overall, this analysis demonstrates that the contrasted daily cycles between the two groups of models imprint on more systematic behaviors of the cloud–convection coupling: In type 1 models, and largely in line with EUREC^{4}A data, i) clouds are more strongly coupled to convection than to the mean RH and ii) cloud transitions are more important than changes in CF_B; whereas in type 2 models, i) clouds depend more on the mean RH than on convection, and ii) CF_B is more variable. Given the evidence that cloud–convection coupling is critical for trade-cumulus feedback, do these contrasted cloud transition behaviors in present-day climate also manifest themselves in different responses to warming?

Trade-Wind Cloud Responses to Global Warming

Fig. 4 *A* and *B* show that models strongly differ in their responses of CF and cloud radiative effect (CRE) to uniform surface warming (*Materials and Methods*). In particular, type 1 and type 2 models differ in their responses of the vertical distribution of CF and of CF_B to global warming. Type 1 models generally simulate a shallowing of the cloud layer, with increased CF near the cloud-base level and decreased CF aloft (Fig. 4*A*). Changes in CF_B are relatively small for type 1 models compared to a larger ensemble of 18 climate models simulations and mostly positive (Fig. 4*B*). Contrastingly, in type 2 models, the changes in cloud depth with warming are small, but cloud responses are more prominent near the cloud-base level with a broad range of amplitudes between $-15\%\ K^{-1}$ and $+10\%\ K^{-1}$ (Fig. 4 *A* and *B*). Fig. 4*B* shows that the predicted responses in CF_B explain about 60% of the intermodel variance in CRE changes.

Mixing-Induced Low-Cloud Feedback. In a warmer atmosphere, assuming unchanged relative humidity and convective mass flux, shallow convection is expected to more efficiently dry the boundary layer by mixing dry free tropospheric air downward because of an increased specific humidity gradient following the Clausius-Clapeyron relation (18, 31–33). All models assessed here exhibit this thermodynamic increase in convective drying (*SI Appendix*, Fig. S7), although with a large range of amplitudes. Given that the convective tendency can be approximated by the product of the mass flux and the MSE gradient (18) (*SI Appendix*, Fig. S11 and *Text*), such a range can be explained by the diversity of mass flux strengths predicted by the models in present-day climate (*SI Appendix*, Fig. S8*C*). The enhanced convective drying with warming can thus produce a cloud amount reduction at a rate that scales with the strength of present-day convective activity, explaining the wide range of low-cloud feedback among models (14, 16).

We show that this mixing-induced drying mechanism could explain the diversity of the cloud responses to warming among most type 2 models but not among type 1 models (*SI Appendix*, Fig. S8*D*). Therefore, and consistently with ref. 21, models underestimating the strength of the cloud–convection coupling (type 2 models in Fig. 3 *C* and *F*) are more prone to simulate a cloud reduction with warming due to mixing-induced drying, whereas models that are closer to EUREC^{4}A observations (type 1 models in Fig. 3 *B* and *E*) tend to produce a weaker cloud-base cloudiness change and thus cloud feedback. In the next section, we show that the convective processes controlling cloud transitions on the daily timescale are at play in response to warming and can explain the weaker trade-cumulus feedback simulated by type 1 models.

Interpretation in Terms of Cloud Type Transition. The analysis of the cloud responses to warming shows that the cloud shallowing in type 1 models is associated with an increased occurrence of very shallow clouds at the expense of deeper clouds (Fig. 4*C*)—similar to the daily transition from night to day. Moreover, the pronounced positive correlation between the +4K cloud transitions and changes in cloud-base cloud fraction (Fig. 4*C*) is consistent with the idea that in a cloud population becoming shallower (thus associated with a shallowing of the convective moisture transport), the moisture brought by the surface is more likely to remain at low levels (rather than being

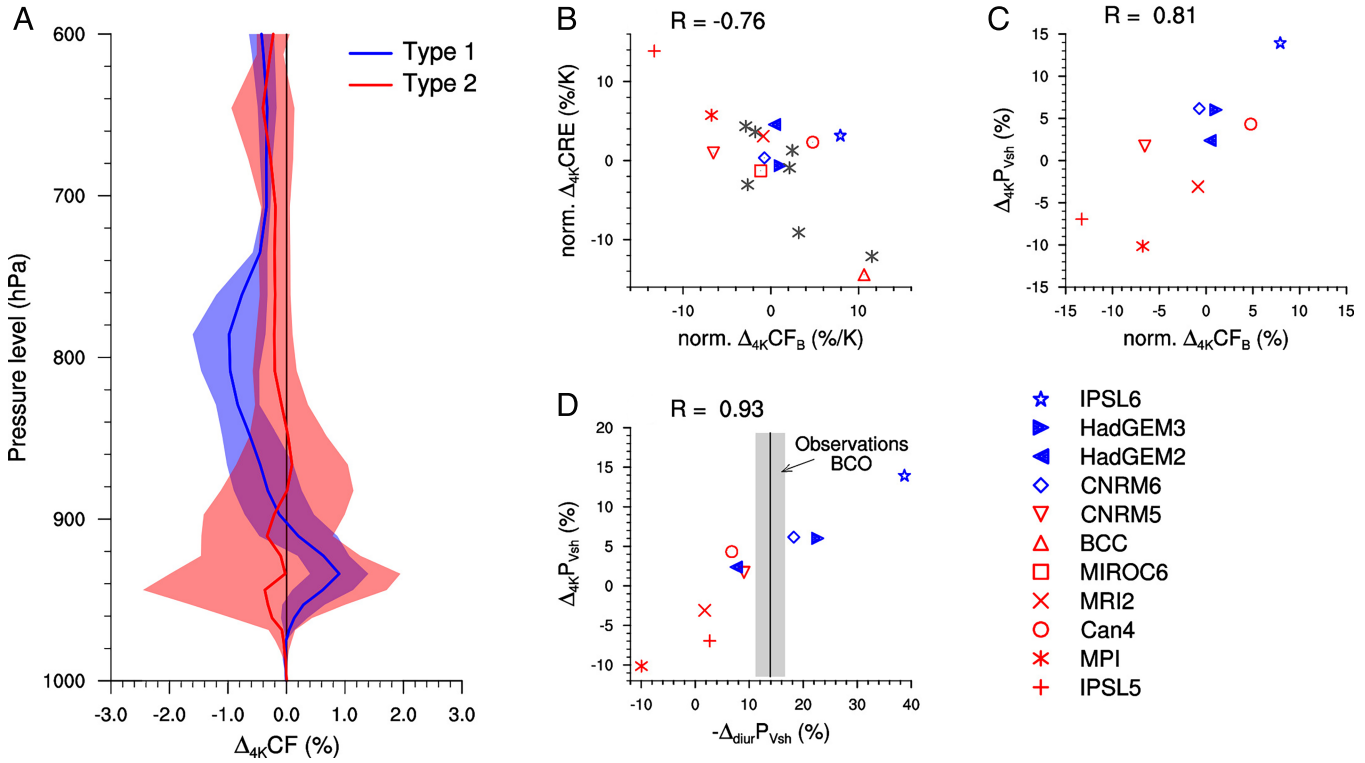

Fig. 4. Diurnal transition of trade-wind cumuli matters for cloud radiative effects changes with warming. (*A*) +4K-changes in CF for type 1 (blue) and type 2 (red) models, with multimodel mean (solid line) and SD (shading). (*B*) +4K-changes in CRE as a function of CF_B, normalized by their respective mean value in the control simulation, for a larger ensemble of 18 climate models (additional models in gray). (*C*) +4K-changes in the proportion of very shallow clouds among all shallow clouds (P_{Vsh}) as a function of normalized +4K-changes in CF_B. (*D*) +4K-changes in P_{Vsh} as a function of daily changes in P_{Vsh} from night to day (between times of daily minimum and maximum CF_B). The vertical black line and shading represent the multiday mean and SE for BCO observations. Note that results in (*A* and *B*) are based on monthly output simulations (Amon), and those in (*C* and *D*) are based on hourly output at selected sites (cfSite).

transported upward by convection) and thus to increase the cloud-base cloudiness.

As shown previously, the propensity of models to simulate cloud transitions depends on how strongly clouds are coupled to convection (Fig. 3 *E* and *F*). In warmer simulations, the convective mass flux weakens and/or shallows in most models (*SI Appendix*, Figs. S7 and S8*B*), which is reflected by shallowing of the convective transport (*SI Appendix*, Fig. S7). Although the response of the shallow convective mass flux to warming is not clearly established (14, 21), one hypothesis could be that the increase in downwelling radiation from the free troposphere (due to the increase in water vapor in a warmer troposphere) helps stabilize the boundary layer to convection (12, 34)—the same mechanism as for the night to day transition in response to a weakened atmospheric radiative cooling.

Given the pronounced correlation between warming-related cloud transitions and daily cloud transitions (Fig. 4*D* and *SI Appendix*, S9), and the better ability of type 1 models to reproduce the observed cloud shallowing as convection weakens at the daily timescale, the cloud shallowing predicted by this group of models under global warming as convection weakens is likely to be more credible. Our findings thus support the behavior of type 1 models, which tend to predict weaker trade cumulus feedback (Fig. 4*B*). They, moreover, make the large responses of some type 2 models less credible.

Summary and Discussion

When analyzing the behavior of trade-cumulus clouds predicted by climate models at the daily timescale, we identify two groups of models. In the first group (type 1), it is mainly the vertical depth of the clouds that changes, as opposed to their horizontal extent, and it covaries with the convective mass flux. Over the daily cycle, a transition occurs in these models from a population of deep trade cumuli during nighttime to a population of very shallow cumuli during daytime, coupled to a weakening of convection at the beginning of the day. Through the same physical mechanism, under global warming, a transition occurs from a deeper to a shallower cloud population as convection weakens with warming. During this transition, the cloud-base cloud fraction varies little, and overall, these models predict a weak trade cumulus feedback.

In the second group (type 2), on the contrary, the models hardly represent cloud transitions in the vertical, and instead, tend to simulate unrealistic stratocumulus-like clouds whose cloud-base extent varies much more with humidity than with the strength of convection. During the night, cloud-base cloud fraction increases as the turbulent diffusive transport strengthens overnight; under climate change, cloud-base cloud fraction decreases, proportionally, through a vertical mixing-induced drying mechanism that leads to strong positive feedback in some models (cf. refs. 14, 16 and 18).

Observations from the Barbados Cloud Observatory and the EUREC^{4}A field campaign indicate that the behavior of type 1 models—exhibiting daily transitions in cloud depth and a stronger coupling of clouds to convection than to humidity—is more credible. In climate models, the simulated cloud–convection relationship is consistent between the daily timescale and global warming. Type 1 models are more credible as assessed by observational constraints and tend to simulate weaker trade

cumulus feedback under warming. This conclusion confirms and reinforces inferences from other observationally based estimates (7, 9, 21), albeit by analyzing different physical processes and different sets of observations.

Many uncertainties in long-term climate projections are rooted in the model representation of fast physical processes, thus emphasizing the importance of evaluating climate models on short timescales (35). The present study provides another demonstration of this: By illuminating the processes that control cloud variations under climate change, the daily cycle appears to be a powerful laboratory for guiding model developments that strongly influence climate change predictions. Most of the climate models considered here simulate unrealistic cloud behaviors at the subdaily timescale. These shortcomings call for a community effort to i) analyze high-frequency model outputs to assess fast physical processes in which many uncertainties of the current climate and future projections are rooted, ii) develop parameterizations that better represent the cloud–convection coupling, the main populations of shallow cumuli observed in nature and their transition on the daily timescale, and iii) better understand the factors that influence the strength of shallow convection, including the role of shallow mesoscale circulations that are ubiquitous in the tropics and have the potential to influence trade cumulus dynamics (21, 26, 36). Addressing these gaps with observations that can be collected every day stands a good chance to ultimately increase the credibility of climate projections.

Materials and Methods

Observations. We use two observational datasets: i) ground-based radar observations from the Barbados Cloud Observatory [BCO, 59.48°W, 13.15°N, (17)] during the boreal winter months (DJFM) from January, 1, 2012, to March, 31, 2021, and ii) in situ and remote sensing measurements from the 1-month EUREC^{4}A field campaign, which took place off the coast of Barbados from January 20 to February 20, 2020 (22, 23).

At BCO, vertical distributions of hydrometeors are derived from two 36-GHz Doppler cloud radars, using all radar returns (cloud and rain droplets) with an equivalent radar reflectivity greater than −50 dBZ. We do not apply any rain correction because periods of rain are usually also periods of cloudiness. Rain-correction has been shown to have a minor impact on the daily cycle of cloudiness (26), but it can account for some of the difference in cloud fraction between BCO and the models (Fig. 1 *A*–*C*). Since the cloud radars have a footprint of a few tens of meters, whereas a model grid-box is about (100 km)^2, we bin the hydrometeor profiles into 1-h averages, which is about the time needed for an air mass to travel across a 25-km distance at 7 m s^{-1}. Results are qualitatively similar when binning data into 4-h averages.

For EUREC^{4}A, we focus on measurements made by the HALO (37) and ATR (38) aircrafts, which flew coordinated 3-h patterns in a ca. 220 -km diameter circle centered at 13.3°N, 57.7°W. The 200-km, 3-h scale of the EUREC^{4}A observations is comparable to the scale that convective parameterizations target. For estimating the cloud-base mass flux M_B and relative humidity, we use dropsonde data from the JOANNE dataset (39). The mass flux is estimated as a residual of the subcloud layer mass budget, as developed by ref. 25 and applied to EUREC^{4}A data in ref. 21. We use the equilibrium $M_B = E + W$, where E is the entrainment rate estimated using a modified version of the classical flux-jump model (40) developed by ref. 41, and W is the mesoscale vertical velocity computed by vertically integrating the divergence of the horizontal wind field measured by the dropsondes (42). See ref. 21 for details and a demonstration of the robustness of the estimate.

The cloud-base cloud fraction CF_B was measured with horizontally staring cloud radar and backscatter lidar from the ATR aircraft flying at the level of maximum cloud base cloud fraction. We use the BASTALIAS lidar-radar synergy product (38), which includes both cloud and drizzle (but not rain). Figure 18 of (38) shows the consistency of this CF_B with complementary and independent estimates in terms of measurement techniques and spatial sampling onboard ATR (38).

To compute the fraction of very shallow versus deeper clouds, we use cloud-top height estimates from the differential absorption lidar WALES onboard HALO (37). We use the 4440 -m and 1540 -m dropsonde levels as representatives for the 600- and 850 -hPa height (representing the campaign-mean heights).

Overall, the dataset used contains twelve HALO flight days with two sets of three 1 h-circles per day. Three 3-circle sets are discarded because of a fraction of clouds deeper than 600 hPa exceeding 0.5% (both sets on February 11 and the second set of February 9), and for one 3-circle set, the WALES lidar was not operating (second set of February 15). For eleven of the remaining 3-circle sets, consistent ATR cloud-base cloud fraction data are available.

GCM Simulations. We use 11 models from the Cloud Feedback Model Intercomparison Projects (CFMIP) and Coupled Model Intercomparison Projects (CMIP), 5 from CFMIP-2/CMIP5 (43, 44), and 6 from CFMIP-3/CMIP6 (45, 46), taking one ensemble member of the atmosphere-only configuration forced by observed sea surface temperatures (SSTs) and sea ice (amip experiment) and selecting the winter-time period (DJFM) from 1979 to 2008. The response of clouds to global warming is assessed from the amip4K experiment, where a uniform warming of 4 K is added to the observed SSTs. We use two types of model outputs: i) monthly gridded outputs (Amon) for the climate change analyses and ii) subhourly outputs at selected sites (cfSite) for the process-scale analyses. In both cases, we focus on oceanic grid points over the North Atlantic trade-wind area (60 to 50°W, 12 to 16°N). For cfSite, this domain includes between 2 and 6 grid point locations depending on models (*SI Appendix*, Table S1), all with similar diurnal characteristics. Note that these models were chosen to allow at least a comparative analysis of the hourly variability of CF profiles (using cfSite outputs) and of the cloud response to warming (using Amon outputs). However, as noted in some figures, output variables can be missing for certain models and/or experiments. We also do not use any radar simulator to compare BCO observations with model outputs as our focus is on qualitative rather than quantitative cloud behaviors.

Definition of Low Clouds, Trade Cumulus Regime, and Daily Cycle. For BCO and the cfSite model outputs, we limit our analysis to shallow convection, by discarding the times when CF above the 600-hPa level (about 4.2 km) is greater than 0.5% (further discussion in *SI Appendix*). We then define two shallow cloud populations as in (24, 26) from hourly cloud profiles: i) the very shallow cloud population when CF below the 850-hPa level (about 1.3 km) is greater than 0.5% and CF between 850 and 600 hPa is lower than 0.5% ii) the deeper cloud population when CF between 850 and 600 hPa is greater than 0.5%, and with no condition for CF below the 850-hPa level, such that it can include clouds with cloud base close to the lifting condensation level or stratiform-like clouds with cloud base above the 850-hPa level. The relative contributions of cloud populations for BCO and the models are shown in *SI Appendix*, Table S1.

The cloud-base level is defined from hourly profiles as the level of maximum cloud fraction between 870 and 970 hPa. If the maximum cloud fraction is smaller than 0.5% for a given profile, the cloud-base level is taken at the climatological level of maximum cloud fraction.

The daily cycle is computed on days when at least 50% of the data are valid (i.e., shallow clouds or clear-sky scenes) during the daytime period (10-19 LT) and during nighttime (22-07 LT) to ensure the occurrence of true transitions between day and night clouds.

The analysis of the changes in response to warming using Amon model outputs is limited to large-scale subsiding regimes, by selecting months and grid points (over the North Atlantic trade-wind region) when the vertical velocity at 500 hPa (ω_{500}) is positive. Although this subsiding regime criterion is rather broad (technically including both shallow cumulus and stratocumulus regimes), it yields a good correspondence of the warming responses with those assessed using cfSite outputs (*SI Appendix*, Fig. S8 *A* and *B*).

Data, Materials, and Software Availability. Models data have been deposited in ESGF; https://esgf-node.llnl.gov. Previously published data were

used for this work. The EUREC^{4}A observations used are openly available through the landing pages of the respective data papers or through the EUREC^{4}A database of AERIS https://eurec4a.aeris-data.fr/. The processed BCO data used and information on how to access the raw data via the BCO intake catalog are available through https://doi.org/10.5281/zenodo.7590265.

ACKNOWLEDGMENTS. We thank all the scientists, engineers, and technicians from the Max Planck Institute for Meteorology and Caribbean Institute for Meteorology and Hydrology in Barbados who have equipped and kept the Barbados Cloud Observatory running since 2010 and all the colleagues from Europe, the United States, and the Caribbean who contributed to the EUREC^{4}A field campaign. Special thanks go to Bjorn Stevens, for his encouragement to use BCO data and stimulating discussions, Julien Delanoë and Patrick Chazette for their help in estimating the cloud-base cloud fraction from the ATR, Martin Wirth for the processing of WALES data, and SAFIRE and DLR for operating the ATR-42 and HALO aircraft during EUREC^{4}A. This research was funded by the European Research Council grant agreement 694768 (ERC Advanced Grant EUREC^{4}A) and the EU Horizon 2020 grant agreement 820829 (CONSTRAIN).

1. N. D. Gordon, S. A. Klein, Low-cloud optical depth feedback in climate models. *J. Geophys. Res.: Atmos.* **119**, 6052–6065 (2014).
2. I. Tan, T. Storelvmo, M. D. Zelinka, Observational constraints on mixed-phase clouds imply higher climate sensitivity. *Science* **352**, 224–227 (2016).
3. J. Bjordal, T. Storelvmo, K. Alterskjær, T. Carlsen, Equilibrium climate sensitivity above 5 °C plausible due to state-dependent cloud feedback. *Nat. Geosci.* **13**, 718–721 (2020).
4. S. Bony, J. L. Dufresne, Marine boundary layer clouds at the heart of tropical cloud feedback uncertainties in climate models. *Geophys. Res. Lett.* **32**, L20806 (2005).
5. J. Vial, J. L. Dufresne, S. Bony, On the interpretation of inter-model spread in CMIP5 climate sensitivity estimates. *Clim. Dyn.* **41**, 3339–3362 (2013).
6. B. Medeiros, B. Stevens, S. Bony, Using aquaplanets to understand the robust responses of comprehensive climate models to forcing. *Clim. Dyn.* **44**, 1957–1977 (2015).
7. T. A. Myers *et al*., Observational constraints on low cloud feedback reduce uncertainty of climate sensitivity. *Nat. Clim. Change* **11**, 501–507 (2021).
8. L. Nuijens, B. Medeiros, I. Sandu, M. Ahlgrimm, The behavior of trade-wind cloudiness in observations and models: The major cloud components and their variability. *J. Adv. Model. Earth Syst.* **7**, 600–616 (2015).
9. G. V. Cesana, A. D. Del Genio, Observational constraint on cloud feedbacks suggests moderate climate sensitivity. *Nat. Clim. Change* **11**, 213–218 (2021).
10. R. Vogel, L. Nuijens, B. Stevens, The role of precipitation and spatial organization in the response of trade-wind clouds to warming. *J. Adv. Model. Earth Syst.* **8**, 843–862 (2016).
11. J. Radtke, T. Mauritsen, C. Hohenegger, Shallow cumulus cloud feedback in large eddy simulations-bridging the gap to storm-resolving models. *Atmos. Chem. Phys.* **21**, 3275–3288 (2021).
12. M. C. Wyant, C. S. Bretherton, P. N. Blossey, Subtropical low cloud response to a warmer climate in a superparameterized climate model. Part I: Regime sorting and physical mechanisms. *J. Adv. Model. Earth Syst.* **1**, 1–11 (2009).
13. A. Gettelman, J. E. Kay, K. M. Shell, The evolution of climate sensitivity and climate feedbacks in the community atmosphere model. *J. Clim.* **25**, 1453–1469 (2012).
14. S. C. Sherwood, S. Bony, J. L. Dufresne, Spread in model climate sensitivity traced to atmospheric convective mixing. *Nature* **505**, 37–42 (2014).
15. L. Tomassini, A. Voigt, B. Stevens, On the connection between tropical circulation, convective mixing, and climate sensitivity. *Q. J. R. Meteorol. Soc.* **141**, 1404–1416 (2015).
16. F. Brient *et al*., Shallowness of tropical low clouds as a predictor of climate models' response to warming. *Clim. Dyn.* **47**, 433–449 (2016).
17. B. Stevens *et al*., The Barbados cloud observatory: Anchoring investigations of clouds and circulation on the edge of the ITCZ. *Bull. Am. Meteorol. Soc.* **97**, 787–801 (2016).
18. J. Vial, S. Bony, J. L. Dufresne, R. Roehrig, Coupling between lower-tropospheric convective mixing and low-level clouds: Physical mechanisms and dependence on convection scheme. *J. Adv. Model. Earth Syst.* **8**, 1892–1911 (2016).
19. M. Zhao *et al*., Uncertainty in model climate sensitivity traced to representations of cumulus precipitation microphysics. *J. Clim.* **29**, 543–560 (2016).
20. N. Hirota *et al*., Underestimated marine stratocumulus cloud feedback associated with overly active deep convection in models. *Environ. Res. Lett.* **16**, 074015 (2021).
21. R. Vogel *et al*., Strong cloud-circulation coupling explains weak trade cumulus feedback. *Nature* **612**, 696–700 (2022) https://doi.org/10.1038/s41586-022-05364-y.
22. S. Bony *et al*., EUREC4A: A field campaign to elucidate the couplings between clouds convection and circulation. *Surv. Geophys.* **38**, 1529–1568 (2017).
23. B. Stevens *et al*., EUREC^{4}A. *Earth Syst. Sci. Data* **13**, 4067–4119 (2021).
24. J. Vial *et al*., A new look at the daily cycle of trade wind cumuli. *J. Adv. Model. Earth Syst.* **11**, 3148–3166 (2019).
25. R. Vogel, S. Bony, B. Stevens, Estimating the shallow convective mass flux from the subcloud-layer mass budget. *J. Atmos. Sci.* **77**, 1559–1574 (2020).
26. J. Vial, R. Vogel, H. Schulz, On the daily cycle of mesoscale cloud organization in the winter trades. *Q. J. R. Meteorol. Soc.* **147**, 2850–2873 (2021).
27. A. C. M. Savazzi, L. Nuijens, I. Sandu, G. George, P. Bechtold, The representation of winds in the lower troposphere in ECMWF forecasts and reanalyses during the EUREC4A field campaign. *Atmos. Chem. Phys. Discuss.* **22**, 1–29 (2022).
28. J. H. Ruppert, R. H. Johnson, On the cumulus diurnal cycle over the tropical warm pool. *J. Adv. Model. Earth Syst.* **8**, 669–690 (2016).
29. R. Wood, Stratocumulus clouds. *Mon. Weather Rev.* **140**, 2373–2423 (2012).
30. S. Bony, K. A. Emanuel, A Parameterization of the cloudiness associated with cumulus convection; evaluation using TOGA COARE data. *J. Atmos. Sci.* **58**, 3158–3183 (2001).
31. M. Rieck, L. Nuijens, B. Stevens, Marine boundary layer cloud feedbacks in a constant relative humidity atmosphere. *J. Atmos. Sci.* **69**, 2538–2550 (2012).
32. P. N. Blossey *et al*., Marine low cloud sensitivity to an idealized climate change: The CGILS LES intercomparison. *J. Adv. Model. Earth Syst.* **5**, 234–258 (2013).
33. C. S. Bretherton, P. N. Blossey, C. R. Jones, Mechanisms of marine low cloud sensitivity to idealized climate perturbations: A single-LES exploration extending the CGILS cases. *J. Adv. Model. Earth Syst.* **5**, 316–337 (2013).
34. M. J. Webb, A. P. Lock, Coupling between subtropical cloud feedback and the local hydrological cycle in a climate model. *Clim. Dyn.* **41**, 1923–1939 (2013).
35. M. J. Rodwell, T. N. Palmer, Using numerical weather prediction to assess climate models. *Q. J. R. Meteorol. Soc.* **133**, 129–146 (2007).
36. G. George, B. Stevens, S. Bony, R. Vogel, A. K. Naumann, Ubiquity of shallow mesoscale circulations in the trades and their influence on moisture variance (2022).
37. H. Konow *et al*., EUREC^{4}A's HALO. *Earth Syst. Sci. Data* **13**, 5545–5563 (2021).
38. S. Bony *et al*., EUREC4A observations from the SAFIRE ATR42 aircraft. *Earth Syst. Sci. Data* **14**, 2021–2064 (2022).
39. G. George *et al*., JOANNE: Joint dropsonde observations of the atmosphere in tropical North Atlantic meso-scale environments. *Earth Syst. Sci. Data* **13**, 5253–5272 (2021).
40. D. K. Lilly, Models of cloud-topped mixed layers under a strong inversion. *Q. J. R. Meteorol. Soc.* **94**, 292–309 (1968).
41. A. L. Albright, S. Bony, B. Stevens, R. Vogel, Observed subcloud-layer moisture and heat budgets in the trades. *J. Atmos. Sci.* **79**, 2363–2385 (2022).
42. S. Bony, B. Stevens, Measuring area-averaged vertical motions with dropsondes. *J. Atmos. Sci.* **76**, 767–783 (2019).
43. S. Bony *et al*., CFMIP: Towards a better evaluation and understanding of clouds and cloud feedbacks in CMIP5 models. *Clivar Exchanges* **56**, 20–22 (2011).
44. K. E. Taylor, R. J. Stouffer, G. A. Meehl, An overview of CMIP5 and the experiment design. *Bull. Am. Meteorol. Soc.* **93**, 485–498 (2012).
45. V. Eyring *et al*., Overview of the Coupled Model Intercomparison Project Phase 6 (CMIP6) experimental design and organization. *Geosci. Model Dev.* **9**, 1937–1958 (2016).
46. M. J. Webb *et al*., The Cloud Feedback Model Intercomparison Project (CFMIP) contribution to CMIP6. *Geosci. Model Dev.* **10**, 359–384 (2017).